Structure of Aggregates of P4BCMU in Dilute THF/Toluene Solutions

Yingjie Li† and Benjamin Chu*,†,‡

Chemistry Department, State University of New York at Stony Brook, Long Island, New York 11794, and Department of Materials Science and Engineering, State University of New York at Stony Brook, Long Island, New York 11794

Received January 7, 1991; Revised Manuscript Received March 6, 1991

ABSTRACT: The aggregation behavior of P4BCMU in THF/toluene mixed solvent was studied by using absorption spectra and both static light scattering (SLS) and dynamic light scattering (DLS). The transition of single molecular coils to stretched-chain aggregates could be described approximately by the Avrami equation. Two different molecular weights of P4BCMU and different mixed-solvent composition were used to investigate the structure of aggregates of P4BCMU by using a combination of SLS and synchrotron small-angle X-ray scattering (SAXS). Based on a semiquantitative comparison of the angular distribution of scattered intensity with a variety of theoretical scattering form factors, the structure of the P4BCMU aggregates can best be described by ribbonlike unsymmetrical elliptic cylinders under all the conditions of our measurements.

I. Introduction

Polydiacetylenes are a series of conducting polymers, which have been the subject of intensive research efforts.[1] In particular, it was found that one of the soluble substituted polydiacetylenes, P4BCMU ($(=CRC\equiv CCR'=)_n$ with R = R′ = $(CH_2)_4OCONHCH_2COOC_4H_9$) has very interesting and unique solution properties.[2] In a good solvent, e.g., chloroform, the color is yellow and the conformation was found to be single-molecular wormlike coils. In poor solvents, e.g., when toluene was added to the P4BCMU in chloroform solution, the color of the solution changed gradually from yellow to red. The conformation in red toluene solution was found to be stretched-chain aggregates with a very narrow size distribution.[2] Although a variety of techniques have been used to study the phenomena, the structure of P4BCMU in toluene could not be determined unambiguously, mainly due to the very low overlap concentration of the particles in the solution ($C^* \approx 2 \times 10^{-4}$ g/mL if $C^* \approx 2^{3/2}M_w/(N_AL^3)$[3,4]). Without an absolute molar mass determination of P4BCMU in toluene, the question whether P4BCMU exists as single molecules or as aggregates remains somewhat open. The molar mass of P4BCMU in toluene could not be determined because the refractive index increment (dn/dc) could not be measured unambiguously at $C < C^*$.[5]

Light scattering intensity experiments could be used to investigate the overall size of the aggregates in terms of the radius of gyration due to its accessible small q values, where $q = 4\pi n/\lambda_0 \sin(\theta/2)$ with λ_0, n, and θ being the wavelength of (visible) light in vacuo, the refractive index of the solution, and the scattering angle, respectively. The internal structure of P4BCMU in toluene could be investigated by means of small-angle X-ray (or neutron) scattering, where $qR_g \gg 1$.[6] By combining measurements of synchrotron small-angle X-ray scattering (SAXS) at the National Synchrotron Light Source (NSLS), Brookhaven National Laboratory (BNL), and laser light scattering at Stony Brook, we were able to determine the structure of the aggregates of P4BCMU in solution semi-quantitatively. In our analysis, a traditional route was followed; i.e., we calculated the scattering form factors of a variety of theoretical models, compared them with our experimental results, and then proposed a most likely structure for the aggregates.

In an earlier paper,[7] we reported our preliminary results that the aggregates of P4BCMU ($M_w = 2.4 \times 10^6$) in pure toluene could be described by a bunching of 14 parallel rods in an 1 row × 14 columns arrangement. In this paper, we present the experimental findings based on the scattering profiles of P4BCMU aggregates with two different molecular weights and in a range of solvent composition using tetrahydrofuran (THF) as the good solvent and toluene as the poor solvent. Semidilute solution properties of P4BCMU in THF/toluene mixed-solvent solution have been reported by Peiffer et al.[8] Absorption spectrum as well as static and dynamic laser light scattering measurements were used to study the time dependence of the aggregation process of P4BCMU. Synchrotron SAXS experiments were then carried out in order to cover a broader SAXS q range not accessible with visible light. In comparison with our earlier SAXS experiments, the SAXS q range has been increased from 5.5×10^{-2}–1.3×10^{-1} to 4.4×10^{-2}–3.0×10^{-1} nm^{-1}.

II. Experimental Section

II.1. Sample and Solution Preparations. Two P4BCMU samples with weight-average molecular weights of 1.2×10^5 and 2.4×10^6 were obtained, courtesy of Drs. R. R. Chance and D. G. Peiffer at the Corporate Research Science Laboratory, Exxon Research and Engineering Co. They were used as-received without further purification. A more detailed description of the samples is available in ref 2.

Tetrahydrofuran (THF) (instead of chloroform) was chosen as a good solvent for this study because it has a relatively low electron density. Toluene was chosen as the second component of the mixed solvent because it is not a nonsolvent like hexane, which has an even lower electron density. A poor solvent instead of a nonsolvent was used in order to avoid possible complications in localized precipitations, which might take longer times for the aggregates to reach equilibrium.

The solution preparation procedure is the same as that in ref 2.

II.2. Absorption Spectrum. Absorption measurements in the wavelength from 350 to 650 nm were performed by using a GCA/McPherson 700 Series double-beam UV–visible spectrophotometer. Mixed solvents with the same composition as that

* Author to whom all correspondence should be addressed at the Chemistry Department.
† Chemistry Department.
‡ Department of Materials Science and Engineering.

0024-9297/91/2224-4115$02.50/0

in the solutions were used as a reference standard. All the experiments were performed at 24 ± 2 °C.

II.3. Laser Light Scattering. Static light scattering (SLS) and dynamic light scattering (DLS) experiments were performed by using a laboratory-made, fully computer-controlled laser light scattering spectrometer, which had a 50-mW He–Ne laser operating at λ_0 = 632.8 nm. A Brookhaven Instruments BI2030AT 72 channel correlator was used to record the intensity–intensity time correlation function. All the experiments were done at 24 ± 2 °C.

At very dilute solution concentrations, the excess Rayleigh ratio with vertically polarized incident and scattered light, R_{vv}, can be related to the weight-average molecular weight M_w and the radius of gyration R_g

$$HC/R_{vv} \approx 1/M_w(1 + q^2R_g^2/3) \quad (1)$$

where $R_{vv} = [(I_u - I_v)/I_{bz}]R_{bz}(n/n_{bz})^2$; I_u, I_v, and I_{bz} are the scattered intensities of solution, solvent, and benzene, respectively; R_{bz} is the Rayleigh ratio of benzene; n and n_{bz} are the refractive indexes of solution and benzene, respectively; and H is an optical constant. In terms of measured intensities, we have

$$I_{bz}/(I_u - I_v) \approx [R_{bz}n^2/(HCM_wn_{bz}^2)](1 + q^2R_g^2/3) \quad (2)$$

Therefore, from a plot of $I_{bz}/(I_u - I_v)$ versus q^2, we get R_g = [3(slope)/(intercept)]$^{1/2}$, which is independent of the refractive index increment (dn/dc).

In DLS experiments, the cumulants method was used to get the average line width, $\bar{\Gamma}$.[10] After extrapolation to zero scattering angle and infinite dilution, $\bar{\Gamma}/q^2$ can be related to the z-average translational diffusion coefficient[11] $\lim_{\substack{C\to 0\\ q\to 0}} \bar{\Gamma}/q^2 = \bar{D}_0°$. Then the hydrodynamic radius, R_h, can be obtained by using the Stokes–Einstein relation $R_h = k_BT/(6\pi\eta\bar{D}_0°)$ where k_B is the Boltzmann constant, T is the absolute temperature, and η is the viscosity of the solvent.

The refractive index of the mixed solvent as a function of the mole fraction of THF was calculated according to the Gladstone–Dale equation.[12] The viscosity of the mixed solvents is calculated to a first-order approximation by a linear addition of viscosity of each individual solvent.

II.4. Small-Angle X-ray Scattering. The synchrotron SAXS experiment was performed at the SUNY X3A2 beamline, National Synchrotron Light Source, Brookhaven National Laboratory,[13-15] using a wavelength of 0.154 nm and a Braun linear position-sensitive detector. Desmearing was not necessary because we used a beam size of ~0.1 × 1.5 mm^2 at the sample holder and a sample-to-detector distance of 1.37 m.

A modified Kratky collimator could have achieved a lower q value of ~0.03 nm^{-1} at the SUNY X3A2 beamline. However, due to mirror deterioration at the time of the present runs, the beam after mirror focusing exhibited a higher order vertical divergence than anticipated. We had difficulty getting the scattering angle down to ~1 mrad where parasitic SAXS intensity became appreciable and could not be reduced to anticipated levels. Therefore, another front slit was mounted 720 mm in front of the Kratky entrance slit in order to define a vertical source reference of the incident X-ray beam for the modified Kratky collimator. The front slit had a width of 2.0 ± 0.3 mm. A vacuum pipe was installed between the front slit and the Kratky collimation system. By using this geometry, we were able to reach a scattering angle down to ~1 mrad, corresponding to a q value of ~0.04 nm^{-1} for λ_0 = 0.154 nm. The experiment duration for each SAXS curve was about 2 h each, for the solution and the solvent, respectively, except for the P4BCMU sample with M_w = 1.2 × 10^5 and a concentration of 6 × 10^{-6} g/g in pure toluene, in which case 3-h (instead of 2-h) runs each were used for the solution and the solvent, respectively. At concentrations of ~1 × 10^{-5} g/g only synchrotron SAXS measurements could yield a sufficient signal-to-noise ratio to render the analysis feasible. Similar concentrations were used in laser light scattering and absorption experiments.

III. Results and Discussion

Figure 1 shows the absorption spectra of P4BCMU (M_w = 1.2 × 10^5) at different weight percents of THF in the THF/toluene mixed-solvent system. The measurements were taken 10 days after the solution preparation in order to assure equilibrium of the aggregation process, if any. The absorption spectra are very similar to those of P4BCMU (M_w = 2.4 × 10^6) in chloroform/toluene solvent mixtures.[2] The peak at ~450 nm remained relatively constant with increasing toluene content in the solvent mixture. However, the peak height at ~540 nm increased markedly with increasing toluene content. The solution changed colors from yellow in pure THF, to orange in mixed solvents of THF/toluene, and finally to red in pure toluene, the color of the solid P4BCMU. An increase in amplitude at the 540-nm peak suggested that the conjugation length had been increased; i.e., the macromolecular chain has been straightened.

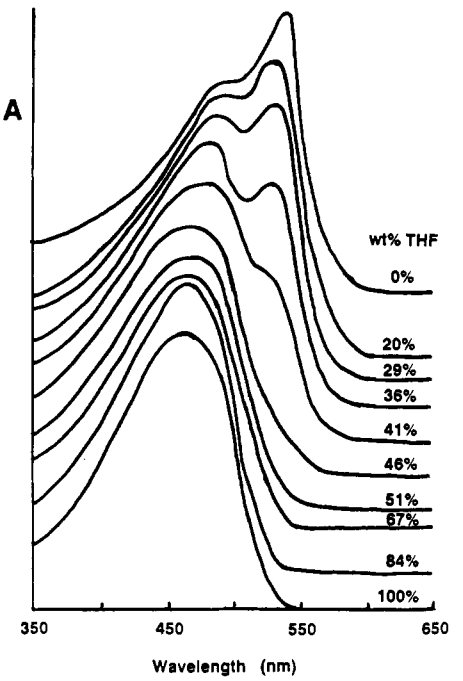

Figure 1. Absorption spectra of P4BCMU (M_w = 1.2 × 10^5) in THF/toluene mixed solvent at different solvent composition. A is absorbance with magnitude displaced in order to reveal peak changes at different weight percents of THF. C is the concentration of P4BCMU, =1 × 10^{-5} g/g.

The time dependence of the structural change is expressed in terms of the normalized ratio of peak amplitudes as shown in Figure 2. The equilibration process became faster with increasing toluene content. The change can be described by the Avrami equation,[16] an equation that can be used to describe the crystallization process of polymers in solution

$$\ln [(Y_\infty - Y_t)/(Y_\infty - Y_0)] = -Zt^n \quad (3)$$

where $Y = A_{540}/A_{450}$, with A being the absorbance; subscripts ∞, t, and 0 denote time at ∞, t, and 0, respectively; and Z and n are constants related to the changing mechanism. Equation 3 suggests that the structural change is very similar to a crystallization process.[17] The values of n decrease with increasing toluene content as listed in the figure caption of Figure 2.

The time dependence of excess scattered intensity of P4BCMU (M_w = 2.4 × 10^6) in THF/toluene mixed solvent with X_{THF} = 36% and C = 1 × 10^{-5} g/g, after extrapolation to the zero scattering angle, is shown in Figure 3. It suggested a trend similar to that observed in the absorption experiment. However, the constant n in eq 3 became 1.0, which was different from that listed in Figure 2, i.e., n = 0.43 from absorption measurement. One may imply that

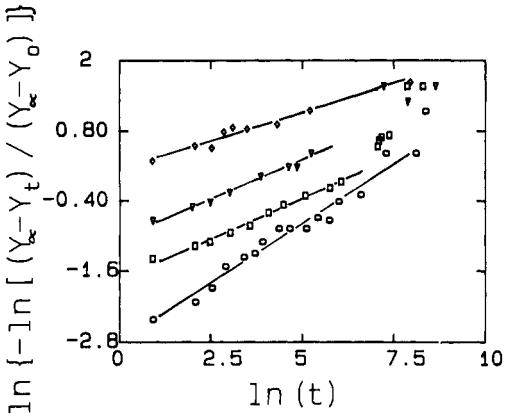

Figure 2. Time dependence of the absorption peak at 540 nm for P4BCMU ($M_w = 1.2 \times 10^5$) at different solvent composition. $Y = A_{540}/A_{450}$ where A_{540} and A_{450} are, respectively, the absorbance at 540 and 450 nm; Y_0, Y_t, and Y_∞ are values of Y at time 0, t, and ∞ after solution preparation, respectively. $C = 1 \times 10^{-5}$ g/g: (◇) $X_{THF} = 20\%$. Least-squares fitting of the data gave a slope of 0.19. (▽) $X_{THF} = 25\%$, Least-squares fitting of the first 8 data points gave a slope of 0.26. (□) $X_{THF} = 29\%$. Least-squares fitting of the first 10 data points gave a slope of 0.27. (○) $X_{THF} = 36\%$. Least-squares fitting of the first 16 data points gave a slope of 0.43. X_{THF} is the weight percent of THF in the mixed solvents.

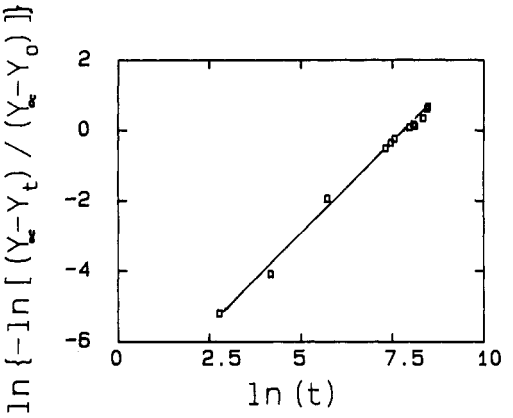

Figure 3. Time dependence of the scattered intensity of P4BCMU ($M_w = 2.4 \times 10^6$) in THF/toluene mixed solvent with $X_{THF} = 36\%$ and $C = 1 \times 10^{-5}$ g/g: (□) I is the scattered intensity with vertical polarization in the incident beam and the scattered beam. I_0, I_t, and I_∞ are values of I ($\equiv Y$) at time 0, t, and ∞ after solution preparation, respectively. Least-squares fitting gave a slope of 1.0.

absorption and scattering are observing different types of changes in the process, but further studies are suggested.

The size of the aggregates, as characterized by the apparent R_g and R_h values, is shown in Figure 4. In the initial process soon after solution preparation, R_g and R_h had approximately the same value, implying a very anisotropic particle shape. As the aggregation process progressed, R_h remained essentially unchanged while R_g showed a slight increase. Therefore, the R_g/R_h ratio increased with increasing time. Here we refer the R_g and R_h values as apparent ones because the light scattering measurements were performed at finite concentrations, without extrapolation to infinite dilution. However, at $C \sim 10^{-5}$ g/g, the R_g and R_h values should be fairly close to the values at infinite dilution. Chu and Xu,[18] considered the overall coil-to-rod aggregate transition as controlled by the slower aggregation process since the number of aggregates increased slowly while the size of the aggregates remained unchanged.

By combining our experimental results from the absorption spectrum, SLS and DLS, we can conclude that

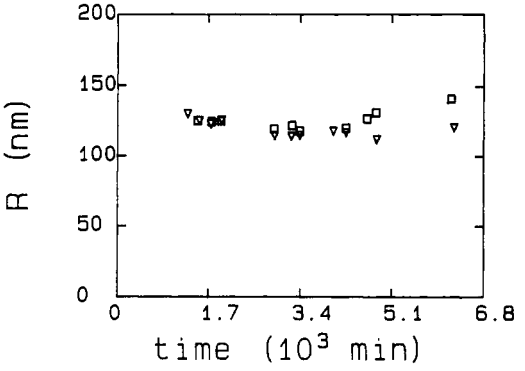

Figure 4. Time dependence of the particle size of P4BCMU ($M_w = 2.4 \times 10^6$) in THF/toluene mixed solvent with $X_{THF} = 36\%$ and $C = 1 \times 10^{-5}$ g/g: (□) radius of gyration, R_g; (▽) hydrodynamic radius, R_h. Both R_g and R_h have estimated relative uncertainties of ~10%. The uncertainties in R_h are higher than usual in view of the relatively short times available for the time-resolved DLS measurements. SLS measurements were performed from $\theta = 15°$ to $\theta = 135°$. DLS measurements were performed at $\theta = 20°$, 30°, 60°, and 90° in order to obtain R_h. No concentration extrapolation was performed.

the molecular chains remain straightened even after the aggregate formation. The R_g/R_h ratio changes could be interpreted according to a fringed micelle model of the aggregates, first proposed by Rawiso et al.[19] Once part of the molecular chain is straightened, an aggregate can form. However, this aggregate has a very condensed, ordered center associated with some flexible, unstraightened chains at the end. While the flexible ends do not contribute as much as the condensed part to the R_g value, it does contribute to the hydrodynamic radius, R_h. The end chains could get straightened later, get attached together, and become as condensed as the aggregated portion of the chain(s). A few more molecules may then attach to the ends of the aggregate, giving rise to an increased R_g value.

Figure 5 shows the size of aggregates as a function of composition of the mixed solvent. In pure toluene the radius of gyration of the aggregates reached ~260 nm. The size of aggregates decreased with decreasing toluene (poor solvent) content. Xu and Chu[2] used a variety of models to fit their experimental data of P4BCMU ($M_w = 2.4 \times 10^6$) in a chloroform/toluene mixed-solvent system. They found that only rods could give reasonable fitting to the measured data. In the present article, different models were used to fit the LS data of R_g and R_h. The LS data of P4BCMU in the THF/toluene mixed solvent also supported a rodlike structure.

Synchrotron SAXS experiments in combination with SLS were used to investigate the P4BCMU structure in mixed solvents of different solvent composition. The excess scattered intensity for a system of particles can be expressed as

$$I(q) = ACMP(q)\,S(q) \qquad (4)$$

where A is a constant with different values for LS and SAXS, C and M are the concentration and molar mass of the particles, respectively, $P(q)$ is the scattering form factor, and $S(q)$ is the structure factor. The form factor depends upon the shape, size, and q value. The structure factor becomes unimportant in the present analysis because our calculation based on the hard-sphere approximation gave the value of $S(q) = 1.0$ with fluctuations below 1% for the q range of both LS and SAXS, at very dilute solution concentrations. The polydispersity effect is also unimportant because the CONTIN analysis[20] of the autocorrelation function from dynamic laser light scattering of

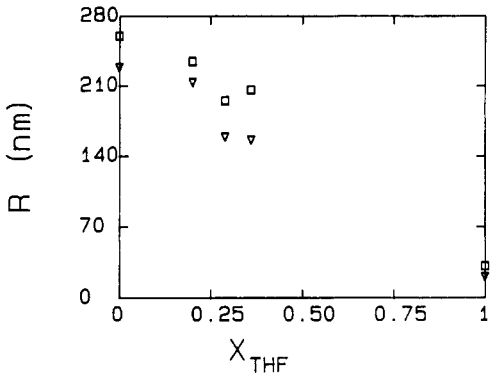

Figure 5. Particle size of P4BCMU ($M_w = 1.2 \times 10^5$) in THF/toluene mixed solvent: (□) radius of gyration, R_g; (▽) hydrodynamic radius, R_h. Both R_g and R_h have estimated relative uncertainties of ~10%.

P4BCMU in pure toluene and in mixed solvent with a high toluene content showed the aggregates to have very narrow size distributions. The variance was only 0.02–0.1. The constant A can be determined by using a reference standard for the absolute scattering intensity. In the present context, we are interested in the shape of the scattering curve in a log–log plot of I vs q. Thus the magnitude of A is no longer an issue. A traditional way to gain structural information is to compare the scattering curve with theoretically calculated form factors of scatterers of assumed geometrical shapes. In order to make the computation, the scattering data from LS, for example, R_g, R_h, and their ratio, can be used as the boundary conditions that the theoretical model must satisfy.

In the paper,[7] we proposed a preliminary aggregate structure consisting of an array of 1 row × 14 columns of individual P4BCMU polymer chains. The average aggregation number was ~14 for P4BCMU with $M_w = 2.4 \times 10^6$.[2] However, for the P4BCMU sample with $M_w = 1.2 \times 10^5$, the average aggregation number is ~360.[2] Thus, the old approach cannot be followed. Another problem involved with the approach used in the paper in ref 7 is that the average aggregate length is 900 nm while the average P4BCMU chain length is 2200 nm, which means that we have to assume some bending or folding geometry for the polymer chain. By taking into account the precision of our SAXS data, a model was constructed based on the assumption that the aggregate particle is homogeneous in density; i.e., the electron density inside the particle is constant. Based on our LS data, the aggregate particle shape, at least to the first-order approximation, is rodlike. Interparticle interference is negligible at very dilute concentrations. Finally, the aggregates are essentially monodisperse as revealed by DLS measurements.

The equations for the scattering form factor of different particle shapes can be obtained from Mittelbach[21] and Kerker[22] and are expressed as follows.

For a sphere with radius a

$$P(q) = \{3[\sin(qa) - qa\cos(qa)]/(q^3a^3)\}^2 \quad (5)$$

For a thin disk with radius a

$$P(q) = 2[1 - BS_1(2qa)/(qa)]/(q^2a^2) \quad (6)$$

with BS_1 being the Bessell function of the first order.

For a Gaussian coil with radius of gyration R_g

$$P(q) = 2[\exp(-q^2R_g^2) + q^2R_g^2 - 1]/(q^4R_g^4) \quad (7)$$

For an elliptic cylinder with semiaxis a, b, and length l

$$P(q) = \int_0^{\pi/2}\phi_Q\{\sin[(ql\cos\Theta)/2]/[(ql\cos\Theta)/2]\}^2\sin\Theta\,d\Theta \quad (8)$$

where

$$\phi_Q = (2/\pi)\int_0^{\pi/2}4\{BS_1([q^2a^2\cos^2\varphi + q^2b^2\sin^2\varphi]^{1/2})\}^2/[q^2a^2\cos^2\varphi + q^2b^2\sin^2\varphi]\,d\varphi$$

Θ is the angle between the long axis of the elliptic cylinder (also the Z axis) and a vector $\hat{n}$ and φ is the angle between the X axis and the projection of $\hat{n}$ onto the X–Y plane, where $\hat{n} = \hat{I} - \hat{I}_0$, with $\hat{I}$ and $\hat{I}_0$ being the unit vectors, which specify the direction of the scattered and the incident beams.

For a parallelpiped with edge a, b, and length l

$$P(q) = \int_0^{\pi/2}\phi_Q\{\sin[(ql\cos\Theta)/2]/[(ql\cos\Theta)/2]\}^2\sin\Theta\,d\Theta \quad (9)$$

where

$$\phi_Q = (2/\pi)\int_0^{\pi/2}\{\sin[(qa\cos\varphi)/2]/[(qa\cos\varphi)/2]\}^2\{\sin[(qb\sin\varphi)/2]/[(qb\sin\varphi)/2]\}^2\,d\varphi$$

Θ and φ are defined in the same way as in the elliptic cylinder geometry.

For a wormlike chain with contour length L and persistence length ρ, Hermans and Hermans[23] have derived

$$P(q) = 2b\{S_i(x) - (1-\cos x)/x\}/(Lx) + 2bS_i^2(x)\{1 - b(1-y^{L/b})/[L(1-y)]\}/[Lx^2(1-y)] \quad (10)$$

with $x = qb$, $b = 2\rho$, $y = \sin(qb)/(qb)$, and $S_i(u) = \int_0^u(\sin t)/t\,dt$.

It should be noted that the model-fitting approach becomes much less practical and meaningful if (1) the scattering curve does not have very good precision and (2) the system has a broad size distribution that is not very precisely known.[22] The scattering curves of different particle shapes usually show noticeable differences in the high-q range. However, in the same q range the excess scattered intensity could also drop dramatically, resulting in lower precision in the measured scattering pattern. This difficulty is further compounded by the size distribution of the system. We have calculated several scattering form factors for polydisperse systems. We note that, by adjusting the parameters in the polydisperse size distribution, we could get very similar scattering curves of fairly different particle shapes. For example, our computer calculation could demonstrate an overlap of the scattering patterns between a monodisperse ellipsoid of revolution and polydisperse spheres. Fortunately, the P4BCMU aggregates in poor solvent have a very narrow size distribution. Our calculation could show that the scattering form factor *including* the measured polydispersity effect became indistinguishable from the one without the polydispersity effect (for more details, see Appendix B). However, due to the relatively low precision of our SAXS data in the high-q range, even when a synchrotron X-ray source was used, the conclusion on the shape of the aggregates is only semiquantitative in nature.

Figure 6 shows some of the theoretically calculated scattering curves of particles with different shapes but basically the same R_g value. It can be seen that the most

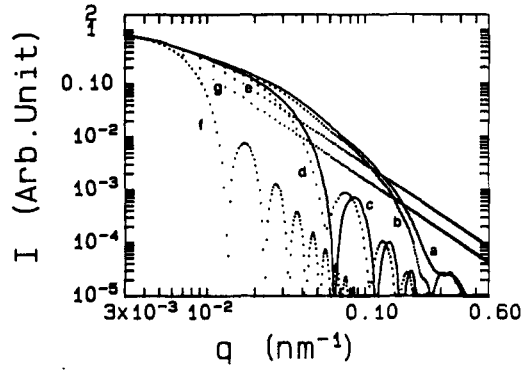

Figure 6. Theoretical scattering form factors of (a) an elliptic cylinder with semiaxis a = 60 nm, b = 13 nm, and length l = 900 nm (R_g = 262 nm); (b) a parallelpiped with edge a = 120 nm, b = 26 nm, and l = 900 nm (R_g = 262 nm); (c) a circular cylinder with radius r = 60 nm, length l = 900 nm (R_g = 263 nm); (d) a parallelpiped with edge $a = b$ = 120 nm, l = 900 nm (R_g = 264 nm); (e) a Gaussian coil with R_g = 260 nm; (f) a sphere with R_g = 260 nm; (g) a disk with R_g = 260 nm.

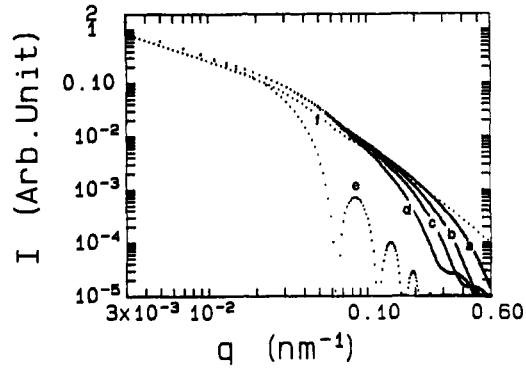

Figure 7. Theoretical scattering form factors of (a) an elliptic cylinder with a = 50 nm, b = 5 nm, l = 900 nm (R_g = 261 nm); (b) an elliptic cylinder with a = 50 nm, b = 7 nm, l = 900 nm (R_g = 261 nm); (c) an elliptic cylinder with a = 50 nm, b = 9 nm, l = 900 nm (R_g = 261 nm); (d) an elliptic cylinder with a = 50 nm, b = 12 nm, l = 900 (R_g = 261 nm); (e) an elliptic cylinder with a = 50 nm, b = 50 nm, l = 900 nm (R_g = 262 nm); (f) 14 parallel rods in a 1 row × 14 columns configuration, with the radius of each rod being 2 nm, the center-to-center distance being 7 nm, and the length l being 900 nm (R_g = 261 nm).

isometric particles give the steepest scattering curves. As the particles become anisotropic in shape, the scattering curves decay more slowly with increasing q. Another feature is that the difference in the triaxial ratio gives rise to the most obvious difference in the scattering curves in the SAXS q range, confirming why SAXS should be used to determine the detailed structure of the aggregates in the present case. Subsidiary maxima of the scattering curves are useful in distinguishing the particle shapes because of their strong dependence upon the particle shape. Unfortunately, at very dilute solution concentrations, the scattering curve could not yield a substantial number of maxima even with synchrotron SAXS.

Figure 7 shows the dependence of the cross-section shape of the elliptic cylinders upon the scattering curves. All the particles have basically the same R_g. The scattering curve decays faster with a more symmetrical cross-section of the scatterer. The scattering behaviors of a series of arrays of individual polymer chains with R_g = 261 nm are shown in Figure 8.

Figure 9 shows the composite excess scattered intensity of P4BCMU (M_w = 2.4 × 10^6 and denoted by hollow squares) in pure toluene, together with the theoretically calculated scattering form factor (solid line) of an elliptic cylinder with semiaxis a = 50 nm, b = 9 nm, and length

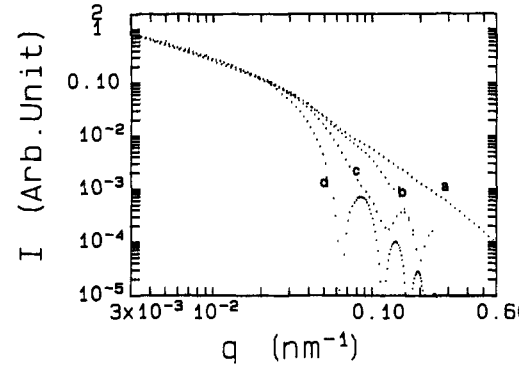

Figure 8. Theoretical scattering form factors of (a) 14 parallel rods in an array of 1 row × 14 columns, with the diameter of each rod being 4 nm and the center-to-center distance being 7 nm; (b) 14 parallel rods in an array of 2 rows × 7 columns, with the diameter of each rod being 8 nm and the center-to-center distance being 15 nm; (c) 15 parallel rods in an array of 3 rows × 5 columns, with the diameter of each rod being 8 nm and the center-to-center distance being 20 nm; (d) one rod with a diameter of 120 nm. In all cases, the length is 900 nm, and the R_g values are 261 nm.

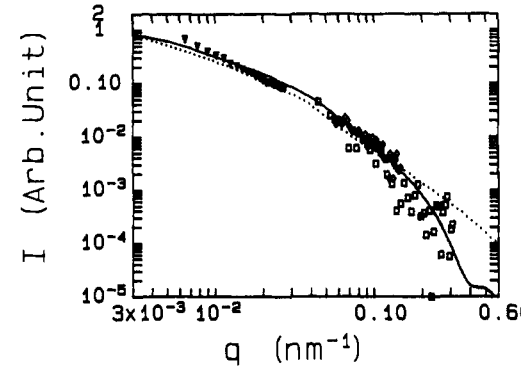

Figure 9. Composite scattering pattern of P4BCMU (M_w = 2.4 × 10^6) in pure toluene with C = 6 × 10^{-6} g/g: (▽) LS. (□) SAXS. (◇) SAXS published in ref 7. Solid line: form factor of an elliptic cylinder with a = 50 nm, b = 9 nm, and l = 900 nm, yielding R_g = 261 nm. Dashed line: form factor of 14 parallel rods in an array of 1 row × 14 columns, with the diameter of each rod being 4 nm, the center-to-center distance being 7 nm, and the length being 900 nm, yielding R_g = 261 nm. It should be noted that the SAXS data (□) fluctuated more than the published SAXS data (◇) mainly because we did not spend sufficient time to accumulate the necessary photon counts due to limited synchrotron time assigned.

l = 900 nm (yielding R_g = 261 nm from the equation $R_g = [(a^2 + b^2)/4 + l^2/12]^{1/2}$). The experimental LS and SAXS data have been shifted vertically in order to compare them with the theoretical form factor. Such shifts do not change the shape of the scattering curve; i.e., only constant A in eq 4 was adjusted for LS and SAXS data. In comparison with our composite experimental data, most of the models could be excluded immediately; for example, a sphere, disk, coil, circular rod, and parallelpiped with a square cross-section do not fit our scattering data. It then becomes necessary to consider the possibility that the cross-section of the particle is not isometric. Both an elliptic cylinder and a parallelpiped with unsymmetrical cross-sections showed reasonable fitting to our composite data. The discussions will be based on the analysis of elliptic cylinders. Uncertainties of the signal-to-noise ratio yield $a:b:l$ ratios of (5.5 ± 1.5):1:(100 ± 30) for the elliptic cylinder. The uncertainty range comes from the data uncertainty, which will be discussed in Appendix A.

In Figure 9, the SAXS data from a previous paper[7] are shown as diamonds. The difference between the 1 × 14 array and the elliptic cylinder is amplified at the high-q

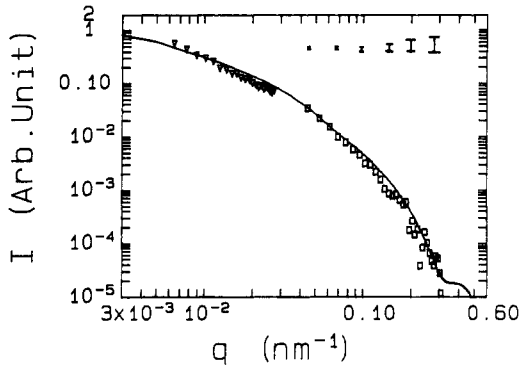

Figure 10. Composite scattering pattern of P4BCMU (M_w = 1.2 × 10⁵) in pure toluene with C = 6 × 10⁻⁶ g/g: (▽) LS. (□) SAXS. "I" denotes experimental error bars based on a detailed error analysis as discussed in Appendix A. Solid line: form factor of an elliptic cylinder with a = 60 nm, b = 11 nm, and l = 900 nm, yielding R_g = 262 nm.

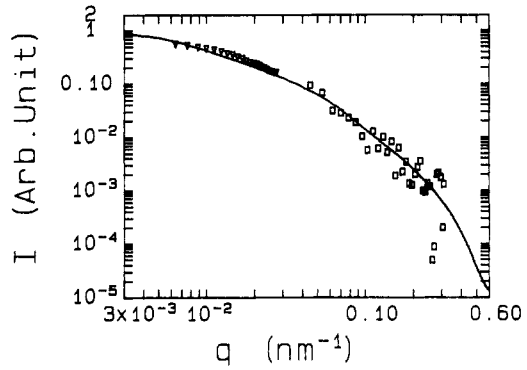

Figure 11. Composite scattering pattern of P4BCMU (M_w = 1.2 × 10⁵) in THF/toluene mixed solvent with X_{THF} = 36% and C = 6 × 10⁻⁶ g/g. (▽) LS. (□) SAXS. Solid line: form factor of an elliptic cylinder with a = 35 nm, b = 6 nm, and l = 700 nm, yielding R_g = 203 nm.

range. Due to the shorter q range of the preliminary synchrotron SAXS data reported earlier,[7] the elliptic cylinder and 1 × 14 array were indistinguishable. The new data covering a broader q range prefer the elliptic cylinder structure.

In order to reach a more decisive conclusion about the P4BCMU (M_w = 1.2 × 10⁵) structure in pure toluene, up to 6 h of accumulation time in combination with a newly injected synchrotron beam was used for the SAXS curve. Figure 10 shows a composite excess scattering pattern of P4BCMU (M_w = 1.2 × 10⁵ and C = 6 × 10⁻⁶ g/g) in pure toluene with a theoretical scattering curve of an elliptic cylinder having a = 60 nm, b = 11 nm, and l = 900 nm (yielding R_g = 262 nm). The structure of the aggregates can be represented by an elliptic cylinder with a:b:l = (5.5 ± 0.5):1:(100 ± 10). Although the P4BCMU (M_w = 1.2 × 10⁵) has a weight-average molecular weight that is 20 times smaller than the higher molecular weight P4BCMU sample (M_w = 2.4 × 10⁶), the structure of aggregates has almost identical shape and dimension. In addition, the size of the aggregates at different concentrations was estimated to remain basically constant at very dilute P4BCMU concentrations. R_g = 260 ± 10 nm from 1 × 10⁻⁵ to 7 × 10⁻⁷ g/g, indicating negligible intermolecular interactions among the aggregates.

Figure 11 shows a composite excess scattering intensity of P4BCMU (M_w = 1.2 × 10⁵) in a THF/toluene mixed solvent with wt % THF = 36%. The theoretically calculated scattering pattern for an elliptic cylinder with a = 35 nm, b = 6 nm, and l = 700 nm (yielding R_g = 203 nm) is denoted by a solid line in Figure 11. a:b:l = (6.0 ± 1.5):1:(120 ± 40). It is interesting to note that, although the particle size in the mixed solvent is smaller when compared with that in pure toluene, the triaxial ratio a:b:l of P4BCMU aggregates is almost identical; i.e., the aggregates have similar shapes.

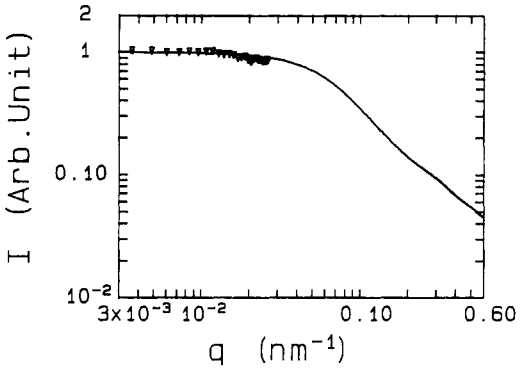

Figure 12. Plot of $I(q)$ for P4BCMU (M_w = 1.2 × 10⁵) in pure THF with C = 6 × 10⁻⁴ g/g: (▽) measured data from LS. Solid line: form factor of a wormlike chain with R_g = 31.2 nm (from LS), contour length L = 120.0 nm (from M_w, M_0, and segment length), and persistence length ρ = 16 nm (from ref 2).

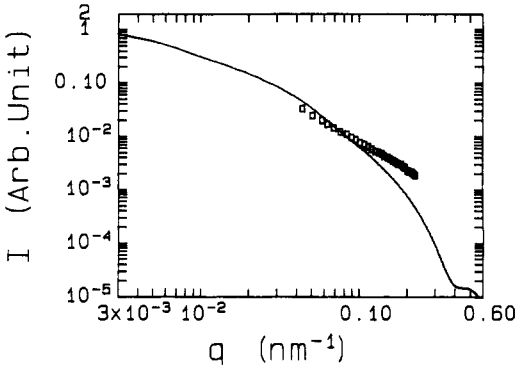

Figure 13. Plot of SANS data (□) of P4BCMU (M_w = 4.32 × 10⁴) in deuterated toluene at 40.5 °C with C = 5.4 × 10⁻⁴ g/g, obtained from Rawiso et al.[23] Solid line denotes a theoretically calculated scattering curve of an elliptic cylinder with a = 50 nm, b = 9 nm, and l = 900 nm (yielding R_g = 261 nm).

The structure of P4BCMU in a good solvent has been found to be wormlike coils.[2] Figure 12 shows a comparison of LS data of P4BCMU (M_w = 1.2 × 10⁵) in pure THF, with the theoretically calculated scattering curve of a wormlike chain[23] having a contour length L of 120.0 nm (from M_w, M_0 = 508, and segment length = 0.48 nm), a persistence length ρ of 16.0 nm, and R_g = 31.2 nm. The R_g/R_h ratio from LS is 1.52. This is a typical value for coils. A R_g/R_h ratio of 1.48 was found when chloroform was used as a good solvent for the same P4BCMU sample. Unfortunately, at C = 6 × 10⁻⁴ g/g, the excess SAXS intensity was less than 100 counts after a total of 4 h of accumulation time.

Figure 13 shows the small-angle neutron scattering (SANS) data[19] of P4BCMU (M_w = 4.32 × 10⁴) in deuterated toluene at 40.5 °C, and the same (as in Figure 9) theoretically calculated scattering curve for an elliptic cylinder having a = 50 nm, b = 9 nm, and l = 900 nm (yielding R_g = 261 nm). It should be noted that the concentration used by Rawiso et al.[19] is much higher, ~5.4 × 10⁻⁴ g/g, when compared with our 6 × 10⁻⁶ g/g. By assuming P4BCMU aggregates in pure toluene to be comparable in size even when these aggregates were prepared from P4BCMU samples of different molecular weight, their concentration was above the estimated overlap concentration of the aggregates with $C^* \approx 2 \times 10^{-4}$

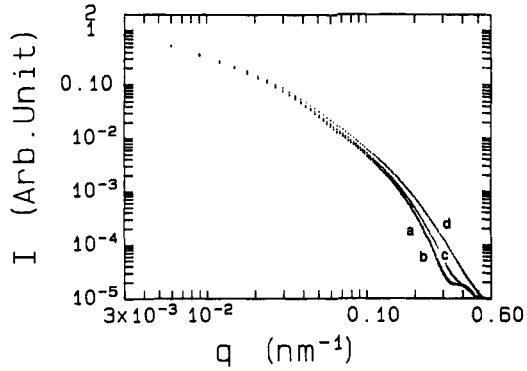

Figure 14. Theoretical scattering form factors of (a) an elliptic cylinder with a = 60 nm, b = 11 nm, and l = 900 nm (R_g = 262 nm); (b) elliptic cylinders with polydispersity being considered based on the DLS and CONTIN analysis (the variance $(\mu_2/\bar{\Gamma}^2)$ = 0.014. The detailed $G(\Gamma)$ distribution will be published separately in the future); (c) elliptic cylinders with polydispersity 3 times broader than the experimental result; (d) elliptic cylinders with polydispersity 5 times broader than the experimental result. Note that curves a and b almost overlap, indicating that the polydispersity effect is not a problem for this system.

g/mL $\approx 2.3 \times 10^{-4}$ g/g even though the molecular weight they used was much lower than ours. These variations could be responsible for the minor discrepancy between the model and the SANS experimental result. If we still use an elliptic cylinder to fit their data, the cross-section would be more unsymmetrical.

IV. Conclusion

The aggregation behavior of the P4BCMU chain upon addition of poor solvent toluene into THF solution can be approximately described by the well-known Avrami equation. The time dependence properties as observed by LS are similar to those in a mixed solvent of chloroform/toluene.[18] The size of the aggregates is dependent upon the mixed-solvent composition. A composite LS and SAXS scattering pattern could be compared with the theoretically calculated scattering behavior of several models, showing that in pure toluene the aggregates from P4BCMU samples with different molecular weight could have comparable size and shape, and in a mixed solvent with X_{THF} = 36%, the aggregates became smaller but still had approximately the same shape. The shape of the aggregates could be described by elliptic cylinders with an unsymmetrical cross-section.

Acknowledgment. B.C. gratefully acknowledges support of this project by the Department of Energy (DE-FG0286-ER45237A005) and the National Science Foundation (DMR8921968). We thank Drs. R. R. Chance and D. G. Peiffer for providing us the samples, and Y.L. thanks Dr. D. Q. Wu, Dr. A. Darovsky, and Mr. W. Lehnert for technical assistance in using the synchrotron SAXS instrumentation and Prof. P. Schmidt, Dr. R. Hilfiker, and Dr. H. Fuchs for helpful discussions.

Appendix A: SAXS Error Analysis

The SAXS data at dilute-solution concentrations often have a low signal-to-noise ratio. A detailed error analysis is useful when we compared the experimental scattering pattern with theoretical models. As LS has a much higher precision than SAXS, the following error analysis is based on the SAXS data only.

The SAXS intensity is proportional to the primary incident intensity $I_0(t)$ (noting that the incident synchrotron X-ray intensity decreases with time), the accumulation time t, the sample thickness d, and the absorption coefficient μ[6]

$$I \sim \bar{I}_0 d \exp(-\mu d) \tag{A.1}$$

where $\bar{I}_0 = \int_0^t I_0(t)\,dt$. By taking into account of the detector nonlinearity and dark count, the excess scattered intensity, I_{ex}, for the polymer solute can be expressed by

$$I_{ex} = (I_s - I_d)\mathcal{L} d_s^{-1} \exp(\mu_s d_s) \bar{I}_{0,s}^{-1} - (I_b - I_d)\mathcal{L} d_b^{-1} \times \exp(\mu_b d_b) \bar{I}_{0,b}^{-1} \tag{A.2}$$

where the subscripts s and b denote solution and solvent, respectively. I_d is the detector dark count, and $\mathcal{L}$ is a calibrated detector nonlinearity factor.

The dark count of a Braun linear position-sensitive detector (LPSD) is negligible. Since the P4BCMU samples did not contain heavy atoms and the concentration used was very dilute with $C \sim 6 \times 10^{-6}$ g/g, the absorption coefficients (μ) for the solution and the solvent are assumed to be the same. The same sample cell was used for both the solution and the solvent experiments. Therefore, $d_s \approx d_b$. It is further assumed that the fluctuations of I_s and I_b obey the Poisson distribution. The relative error in I_{ex} is therefore[24]

$$\sigma(I_{ex})/I_{ex} \approx \{(I_s + I_b) + (I_s^2 + I_b^2)[\sigma^2(\mathcal{L})\,\mathcal{L}^{-2} + \sigma^2(d)\,d^{-2} + \sigma^2(\bar{I}_0)\,\bar{I}_0^{-2}]\}^{1/2}/I_{ex} \tag{A.3}$$

Both the detector nonlinearity correction factor and $\bar{I}_0$ have relative errors of ~5%. The relative error for the thickness is ~10%. Thus we have

$$\sigma(I_{ex})/I_{ex} \approx \{(I_s + I_b) + 0.015(I_s^2 + I_b^2)\}^{1/2}/I_{ex} \approx \{2I_b + 0.03I_b^2\}^{1/2}/I_{ex} \tag{A.4}$$

Four data points were averaged; therefore, we have

$$\sigma(I_{ex})/I_{ex} \approx \{2I_b + 0.03I_b^2\}^{1/2}/\{I_{ex}(4-1)^{1/2}\} \tag{A.5}$$

Based on the above consideration, the relative error for the best SAXS data in Figure 10 could be as large as 1, which would make the conclusion less definitive.

Alternatively, at a high enough q range, the scattered intensity of the solution and that of the solvent may be assumed to become identical; then a different way as has been used successfully by Hilfiker, Wu, and Chu[25] to analyze the SAXS data of a block copolymer system can be used. From eq 8, together with the above discussion

$$I_{ex} = I_s - cI_b \tag{A.6}$$

where

$$c = \{(d_s/d_b)(\bar{I}_{0,s}/\bar{I}_{0,b}) \exp(\mu_b d_b - \mu_s d_s)$$

and

$$\sigma(I_{ex})/I_{ex} \approx \{I_s + c^2 I_b + I_b^2 \sigma^2(c)\}^{1/2} \tag{A.7}$$

Instead of calculating the correction parameter c, we assumed I_{ex} = 0 over a q range from 0.65 to 0.8 nm^{-1} and then calculated the c parameter from the SAXS curves of the solution and the solvent. A total of 20 data points was used to obtain an average value for c. Thus, the relative error for c was further reduced by a factor of $(20-1)^{1/2}$. The relative error for I_{ex} calculated this way was ~5% at q = 0.05 nm^{-1} and ~50% at q = 0.3 nm^{-1} as shown in the upper right corner of Figure 10. The relative error is dependent upon the excess scattered intensity and therefore upon q. The relative errors for all other SAXS data have higher values due to the lower excess scattered intensity (by a factor of ~3). All the SAXS results were analyzed

this way and the effects included in the discussion on the shape of the P4BCMU aggregates.

Appendix B: Effect of Polydispersity on the Scattering Form Factor

For a polydisperse system, the excess scattered intensity can be expressed by

$$I(q) = A\sum F_w(M)\, MP(M,q)\, S(M,q)/\sum F_w(M) \qquad (B.1)$$

where $F_w(M)$ is the weight-average molecular distribution function on the M scale. We need $F_w(M)$ to calculate $I(q)$.

The approximate molar mass distribution of the P4BCMU aggregates in pure toluene was calculated following the method described by Wu et al.[26] because we have two aggregate systems in pure toluene from the two P4BCMU samples with different molecular weights. It is then assumed that, for the aggregates with different molar masses, the size is different, but the a:b:l ratio remains unchanged. Assuming the aggregates with molar mass M_i have size parameters a_i, b_i, and l_i with volume $V_i = \pi a_i b_i l_i$, the aggregates with molar mass M_ν have size parameters νa_i, νb_i, and νl_i with $V_\nu = \pi \nu a_i \nu b_i \nu l_i = \nu^3 V_i$; then the molar mass distribution $F_w(M)$ can be transformed to $F_w(\nu)$ with $\nu^3 = M/M_i$. From $F_w(\nu)$ the distribution of (a,b,l) can be calculated, and eq 9 could be used to calculate the scattering form factor of this polydisperse system. In Figure 14, we can see that our P4BCMU aggregates have little polydispersity effect on the scattering form factor. In order to take into account all the approximations and assumptions we made, we intentionally enlarged the size distribution by a factor of 3 and 5, respectively. From this analysis we can confidently see that the polydispersity effect does not play an observable role in the determination of the aggregate structure.

References and Notes

(1) *Polydiacetylene*; Bloor, D., Chance, R. R., Eds.; NATO Advanced Study Institute Series E; Martinus Nijhoff Publishers: Dordrecht, The Netherlands, 1985; Vol. 102.
(2) See, for example: Xu, R.; Chu, B. *Macromolecules* **1989**, *22*, 3153 and references therein.
(3) Doi, M.; Edwards, S. F. *J. Chem. Soc., Farady Trans. 2* **1978**, *74*, 560, 918.
(4) Ying, Q.; Chu, B. *Macromoleulces* **1987**, *20*, 362.
(5) Muller, M. A.; Schmidt, M.; Wegner, G. *Makromol. Chem., Rapid Commun.* **1984**, *5*, 83.
(6) *Small Angle X-Ray Scattering*; Glatter, O., Kratky, O., Eds.; Academic Press: London, 1983.
(7) Chu, B.; Xu, R.; Li, Y.; Wu, D. Q. *Macromolecules* **1989**, *22*, 3819.
(8) Peiffer, D. G.; Chung, T. C.; Schulz, P. K.; Garner, R. T.; Kim, M. W. *J. Chem. Phys.* **1986**, *85*, 4712.
(9) Huglin, M. B. In *Topics in Current Chemistry*; Springer-Verlag: New York, 1978; Vol. 77, p 141.
(10) Koppel, D. E. *J. Chem. Phys.* **1972**, *57*, 4814.
(11) Stockmayer, W. H.; Schmidt, M. *Pure Appl. Chem.* **1982**, *54*, 407; *Macromolecules* **1984**, *17*, 509.
(12) Huglin, M. B., Ed. *Light Scattering from Polymer Solutions*; Academic Press: New York, 1972.
(13) Philips, J. C.; Baldwin, K. J.; Lehnert, W. F.; LeGrand, A. D.; Prewitt, C. T. *Nucl. Instrum. Methods* **1986**, *A246*, 182.
(14) Chu, B.; Philips, J. C.; Wu, D. Q. In *Polymer Research at Synchrotron Radiation Source*; Russell, T. P., Goland, A. N., Eds.; BNL 51847, UC-25 (Materials-TIC-4500), National Technical Information Service, U.S. Department of Commerce, Springfield, VA, 1985.
(15) Chu, B.; Wu, D.; Wu, C. *Rev. Sci. Instrum.* **1987**, *58*, 1158.
(16) Avrami, M. *J. Chem. Phys.* **1939**, *7*, 1103; **1940**, *8*, 212; **1941**, *9*, 177.
(17) Sperling, L. H. *Introduction to Physical Polymer Science*; John Wiley & Sons: New York, 1986.
(18) Chu, B Xu, R. In *Proceedings of ELECTROPTO88*; Chapter 4, p 177.
(19) Rawiso, M.; Aime, J. P.; Fave, J. L.; Schott, M.; Muller, M. A.; Schmidt, M.; Baumgartl, H.; Wegner, G. *J. Phys. Fr.* **1988**, *49*, 861.
(20) Provencher, S. W. *Comput. Phys. Commun.* **1982**, *27*, 213; **1982**, *27*, 229.
(21) Mittelbach, P. *Acta Phys. Austriaca* **1964**, *9*, 53.
(22) Kerker, M. *The Scattering of Light and Other Electromagnetic Radiation*; Academic Press: New York, 1969.
(23) Hermans, J., Jr.; Hermans, J. J. *J. Phys. Chem.* **1958**, *62*, 1543.
(24) Bevington, P. R. *Data Reduction and Error Analysis for the Physical Sciences*; McGraw-Hill: New York, 1969.
(25) Hilfiker, R.; Wu, D. Q.; Chu, B. *J. Colloid Interface Sci.* **1990**, *135*, 572.
(26) Wu, C.; Zuo, J.; Chu, B. *Macromolecules* **1989**, *22*, 633.

Registry No. P4BCMU, 68777-93-5; THF, 109-99-9; toluene, 108-88-3.